Polymer 51 (2010) 568–580

Contents lists available at ScienceDirect

Polymer

journal homepage: www.elsevier.com/locate/polymer

Rheological control in foaming polymeric materials: I. Amorphous polymers

Ruogu Liao, Wei Yu*, Chixing Zhou

Advanced Rheology Institute, Department of Polymer Science and Engineering, Shanghai Jiao Tong University, Shanghai 200240, PR China

ARTICLE INFO

Article history:
Received 27 September 2009
Received in revised form
10 November 2009
Accepted 30 November 2009
Available online 4 December 2009

Keywords:
Foaming
Long chain branching
Rheology

ABSTRACT

The influence of rheological properties, especially melt strength, on foam structures, such as cell size, cell density and cell size distribution, of amorphous polymer was investigated. The rheology of polystyrene (PS) was controlled by molecular modification with free radical reaction, and PS with long chain branching (LCB) level ranging from 0.15 to 1.6 branching point per 10^4 carbon atom was gotten. The shear and elongational rheology were found to be dependent on the LCB structure, and the strain hardening behavior of modified samples in transient elongational viscosity confirmed the existence of long branched chain. The effects of chain structure and foaming conditions such as temperature and pressure were studied by the analysis on the foam structures obtained by supercritical CO_2. The experimental results revealed that increasing LCB level would decrease cell size, make cell size distribution narrower and slightly increase cell density. The effects of chain topology on the foam structures were also investigated by numerical simulation, where Pom–Pom model was used to describe the effect of backbone length and arm length. The dependence of cell size on the arm length was consistently observed in experiments and simulation. It suggested that the arm length had greater influence on the cell radius than the backbone length. Therefore, the relationship among foam structures, rheological properties and molecular structures can be established from both experiments and simulation, which can be used as a guidance to control the foam structure by designing and controlling the molecular structures and the corresponding rheological properties.

1. Introduction

Polymeric foams typically exhibit high impact strength, toughness and thermal stability, as well as low dielectric constant and thermal conductivity. These unique properties make them ideal for a large number of applications including automotive parts with high strength-to-weight ratio, sporting equipment with reduced weight and high energy absorption, food packaging and insulation with reduced material costs and low dielectric insulators for microelectronic applications [1]. However, the applications of foam are determined by its structure, such as cell type, cell size, cell size distribution and cell density. The foam structures are strongly dependent on the foaming condition [1,2], molecular structure of polymer and corresponding rheological properties [3,4] and components of materials [5,6].

Materials used to foam can be simply divided into two categories: single phase materials (amorphous polymer) and multi-component or multi-phase system (such as polymer blends, polymer with nucleation agents and crystalline polymer etc.). Many factors can affect the foam structures, including the processing conditions and the components or structures of materials. For single phase system, foam structure is often adjusted by foaming condition, such as saturation pressure, foaming temperature and pressure drop rate etc. When foaming using the supercritical CO_2, it is found that higher CO_2 pressure results in smaller cell size and narrower cell size distribution, and higher temperature leads to bigger cell size and broader distribution [1], while higher pressure drop rate results in smaller cell and higher bulk foam density [2]. For multi-phase system, except for foaming condition, many other methods can be used to adjust foam structure. For example, adding nucleation agent is a frequently used and effective technique to reduce cell size, enhance cell density and uniform cell size distribution. As one of the most popular nucleation agents, clay has been used in polypropylene [7,8] and polylactide [6] foaming materials. Generally speaking, the compositions and the multi-phase structures of materials are decisive in controlling foam structure. However, direct connections between the composition/microstructures of materials and foam structure cannot be built up straightforwardly. Missing of such connections could be attributed to the viscoelastic phase separation and possibly multiple phase transitions of foaming process, while rheology is a possible tool to link microscopic and mesoscopic structures with the foam structures.

* Corresponding author. Tel.: +86 21 54743275; fax: +86 21 54741297.
E-mail address: wyu@sjtu.edu.cn (W. Yu).

0032-3861/$ – see front matter © 2009 Elsevier Ltd. All rights reserved.
doi:10.1016/j.polymer.2009.11.063

To understand the role of rheology in foaming, a simple bubble growth model for Newtonian fluid can be illustrative. It shows that the change of bubble radius R is proportional to the pressure difference inside and outside the bubble and inverse proportional to the viscosity of matrix (η) [9]:

$$\frac{dR}{dt} = \frac{R}{4\eta}\left(P_D - P_C - \frac{2\gamma}{R}\right) \quad (1)$$

The value of viscosity determines the process of bubble growth directly, and high viscosity will slow down the speed of bubble growth. However, constant viscosity cannot meet the requirement of controllable foaming. It is desirable that the viscosity is low during nucleation and early stage of bubble growth, increases gradually as the bubbles grow further, and becomes very high in the late stage of foaming to stabilize the foam structures. Such complex time-dependent viscosity could be an indication of the importance of the rheology in foaming process. Although the rheology of polymeric materials can be tuned by many methods like long chain branching, crystallization, blends with rheological modifiers, it is still quantitatively unknown about how to get control on the foam structures by rheology, and furthermore by the microstructures of materials. In this manuscript, the structural and rheological control in amorphous polymer is discussed, and more complex systems with crystallization and multi-components will be included in our future work.

Some efforts have been made to connect the molecular structures with the foam structures. Stafford et al. [3] studied the effects of molecular weight, polydispersity and low molecular weight components on foam structure. They suggested that molecular weight and polydispersity were not important factors in determining cell size and were not responsible for disparity in cell size, while varying the concentration of oligomer allowed control of cell size in foams. Di [4] showed that linear chain extended poly(lactic acid) (PLA) had enhanced melt viscosity and elasticity, and the foam had reduced cell size, increased cell density and lowered bulk foam density in comparison with original linear PLA foam. For branched polymers, Nam et al. [7] and Gotsis et al. [8] had found that the melt strength, elasticity and strain hardening behavior of long chain branched polypropylene increased with LCB level (the number of long chain branches on the main chain), and so did the processability in foaming processes. However, the direct relationship between long chain branching structure and foam structure has not been established.

It has been noticed that a lot of work on the foaming of branched polymers took use of reactive processing method to get the branched structures. However, due to the missing of a direct connection between the branched structure and the foam structures, we are still unaware of how to get well controlled foam structures by making more efficient chemical modification on the polymers. This also pushes us to consider this problem theoretically. Numerical simulations based on the nucleation and bubble growth have been performed [9–12], from which the effects of different processing parameters, such as temperature and pressure, could be determined as a guide for the actual foaming process. In most simulations, description of the rheological properties of polymer is developed from Newtonian fluids [9] to viscoelastic ones [12]. However, phenomenological viscoelastic constitutive equations were used, which are very difficult to connect the chain structures with the foam structures. Moreover, only bubble growth process was considered in most simulations, and a few of them considered the nucleation process. Therefore, it is necessary to consider all the effects, including the chain structures and processing parameters, on the foam structures to illustrate what kind of chain structures are needed for desired foam.

The application of supercritical CO_2 ($scCO_2$) in microcellular foaming processes is an area of significant research activity. As an environment-friendly physical foaming agent, CO_2 has many advantageous properties, including adjustable solvent strength, plasticization, enhanced diffusion rates [1,2] and a moderate critical temperature and pressure. In present work, the amorphous polymer, polystyrene, was chemically modified to obtain different molecular structures and foamed by $scCO_2$. The variations of cell size, cell density and cell size distribution with different LCB levels were recorded. Then the relationship between long chain branching structure and foam morphology was established. At the same time, simulations on the foaming process were performed to establish the connection between the chain structures and the final foam structures. The simulation results were validated by the experimental results, which suggest an effective way to control the foam structures by modifying the chain structures.

2. Experimental

2.1. Materials

Commercial polystyrene (PS), GPPS MC3700 (M_w = 195, 000), was obtained from Chevron Philips Chemical Company, Zhangjiagang city, China. The melt flow rate (MFR) is 3.0g/10 min measured by the method of ASTM D-1238. The samples were stabilized by addition of 0.2 wt% Irganox 1010 (Ciba, Switzerland) antioxidant when they were blended with other reactants. 2, 5-Dimethyl-2, 5(*tert*-butylperoxy) hexane peroxide was obtained from Sinopharm Chemical Reagent Co., Ltd, Shanghai, China, whose half-life time is about 1 min at 180 °C. A kind of multi-functional monomer, pentaerythritol triacrylate (PETA), was obtained from Tianjin Kemao Chemical Reagent Company, China. Both the peroxide and PETA were used as-received. CO_2 (>99.8% purity) was supplied by Chenggong Gas Company, Shanghai, China.

2.2. Experiment procedure

LCB PSs were obtained by modification of commercial PS through reactions in a Haake Rheocord 90 mixer (Thermo Fisher Scientific, Germany) at temperature of 175 °C and a rotational speed of 60 rpm. The formulas of each sample were listed in Table 1. In order to make the additives disperse evenly in PS, they were dissolved in appropriate amount acetone first, and then the solution was added into PS. At last, the mixture was stirred for 5 min and placed in ventilating cabinet at room temperature until the acetone volatilized completely. The mixtures were put into Haake mixer and reacted for 10 min. The products were compressed into pieces of about 1 mm thickness on a hot stage under the pressure of 10 MPa and temperature of 180 °C. The pieces were used for rheological characterization and foaming experiments.

A piece of modified PS was cut into a sheet of 2 cm × 2 cm and put into a self-made autoclave. Then CO_2 was compressed into the autoclave to a certain pressure and then the autoclave was heated to foaming temperature (from 60 °C to 110 °C). The pressure of CO_2

Table 1
Formulation, abbreviation and grafting degree of each sample.

Samples	PS (g)	Irganox1010 (wt%)	Peroxide (wt%)	PETA (wt%)	Carbonyl index	Grafting degree (wt%)
S0	50	0.2	0.1	0	0	0
S2	50	0.2	0.1	0.5	0.31	0.36
S3	50	0.2	0.1	1.0	0.57	0.87
S5	50	0.2	0.1	2.0	0.83	1.40
S8	50	0.2	0.1	4.0	1.29	2.03

was from 7.3 MPa to 14 MPa. After 4 h (complete absorbance of CO_2), the pressure was released at an average speed of about 1 MPa/s. Finally, the products were taken out quickly and put into ice water to freeze the structure of the foams.

2.3. Fourier transform infrared spectroscopy (FTIR)

In order to confirm the grafting of PETA onto the backbone of PS, FTIR was used to test the structure of all samples. At first, the reacted samples were dissolved in hot tetrahydrofuran (THF) at 60 °C. After completely dissolved, the solutions were charged into acetone at room temperature. PS and PS-g-PETA were precipitated out, while the unreacted PETA monomer and polymerized PETA remained in the solution. PS and PS-g-PETA were separated from the solution by filtration, and then dried at 50 °C under vacuum for 24 h. The purified samples were grinded with KBr powder and compressed into films to analyze by Paragon 1000 (PerkinElmer, Inc., USA) infrared spectrometer.

2.4. Rheological measurements

Elongational rheology was carried out on an ARES-RFS rheometer (TA Instruments-Waters LLC, USA) at 180 °C. The size of samples was 17 mm × 10mm × 1 mm. The elongational rate was 0.1, 0.3, and 0.5 s^{-1}, respectively. Frequency sweep was carried out on Gemini 200HR rheometer (Bohlin Instruments, UK) with parallel-plate geometry (diameter is 25 mm). Small amplitude oscillatory shear was performed in the frequency range of 0.01–100 rad/s at 180 °C. A strain of 5% was used, which was in the linear viscoelastic regime for all samples.

2.5. Scanning electron microscopy (SEM)

SEM was used to observe the foam structure. The foamed samples were fractured after being immersed in liquid nitrogen for 30 min (to avoid the deformation or damage of the bubbles). Then the cross-sections were coated with gold and observed on a HITACHI S-2150 scanning electron microscope (Hitachi Corp., Japan). The cell size and cell density were obtained by image analysis software. For statistical accuracy, at least 50 bubbles were tested in one image. Three images were chosen for each sample and the average value was taken as the cell diameter. Because the bubbles in cross section were mostly elliptical or polygonal, the long axis was taken as the diameter of the bubbles. The cell density, N_0, in cells/cm^3 can be determined by Eq. (2):

$$N_f = \left(\frac{nM^2}{A}\right)^{3/2}, \quad V_f = \frac{\pi}{6}D^3 \times N_f, \quad N_0 = \frac{N_f}{1 - V_f} \tag{2}$$

where n is the number of cells on the SEM image, M the magnification factor, A the area of the image (cm^2) and D the cell diameter. Another method to examine foam structure is 3D imaging technique such as X-ray tomography followed by image processing. But it is not used here because of its limited resolution [13].

3. Results and discussion

3.1. FTIR spectroscopy

The FTIR spectra of purified samples are shown in Fig. 1. For S0, there was no PETA added, so the reaction in mixer was just degradation. Its spectra are the same as that of pure PS. While for the other samples reacted with PETA (S2, S3, S5 and S8), there is a band at about 1734 cm^{-1} which is due to the stretching vibration

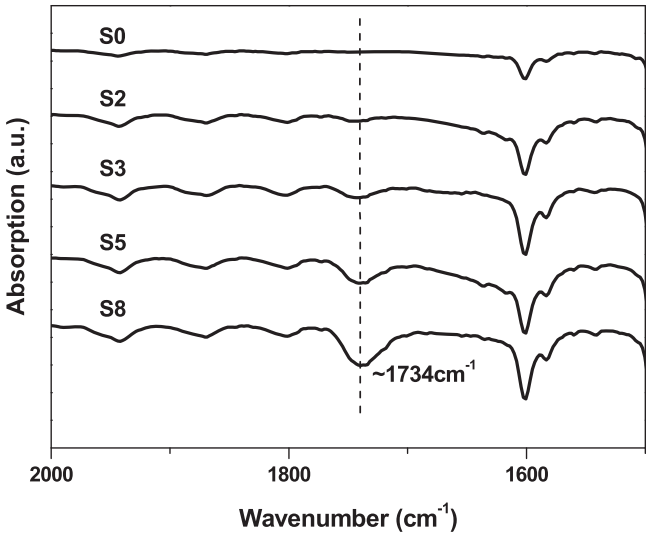

Fig. 1. FTIR spectra (1500–2000 cm^{-1}) of the purified samples.

of the carbonyl group of ester in PETA [14], indicating that PETA was grafted onto the backbone of PS. At the same time, it is found that the intensity of the band increases with the content of PETA. The relative grafting degree can be calculated by carbonyl index (*CI*) from FTIR spectra:

$$CI = \frac{A_{1734}}{A_{835}} \tag{3}$$

where $A_{1734}$is the area of the band at 1734 cm^{-1}, characteristic of carbonyl groups of the ester in the PETA molecules; and A_{835} is that at 835 cm^{-1}, characteristic of benzene ring vibration. *CI* is just a relative value, and in order to get the actual grafting degree, a calibration is needed. The calibration was as follow: the known amount of PETA and PS was dissolved in THF and then the solution was coated on the KBr film. From the FTIR spectra of the latter, the known content of PETA can be corresponded to its CI value. From the calibration curve, the actual grafting degree can be determined and it is listed in Table 1 with *CI*. It can be seen that the grafting degree increases with the content of PETA. This may help in forming more long chain branches on the backbone of PS, which can be confirmed by the enhancement of viscosity and storage modulus (not plotted in this paper) from rheological experiments.

3.2. Determination of LCB

The mechanism of long chain branching formation had been revealed in many papers [15–17]. According to the free radical reaction mechanism, the product is assumed to be a mixture of linear PS and branched PS with long chain branch. Generally, three techniques are often used to test and quantify the level of LCB: ^{13}C NMR, multidetector GPC and rheology technique. However, the former two fail to detect very low level LCB [18,19]. Furthermore, NMR cannot distinguish the chain whose length is longer than six carbon atoms or greater [18]. Rheology technique, on the other hand, is very sensitive to the branched structure and is possible to quantitatively determine the branched structures. Elongational rheology can confirm the existence of LCB by the strain hardening phenomena, while the linear viscoelasticity could be used to quantitatively calculate the level of LCB.

Elongational rheology is one of the most sensitive measurements of LCB [20,21]. When the extensional rate is very low, the elongational viscosity grows slowly and approaches a plateau in

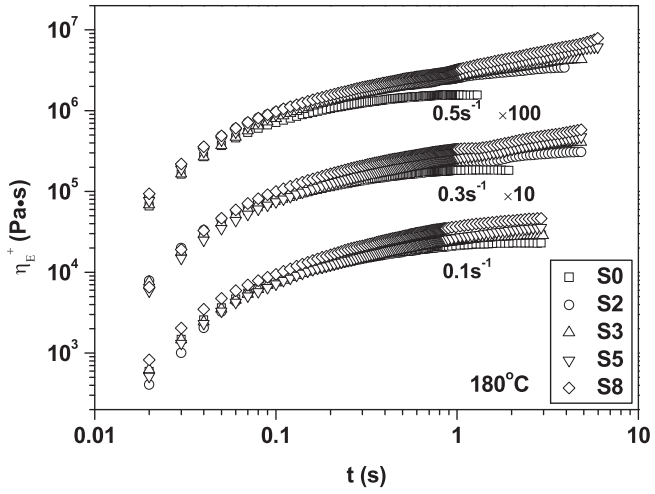

Fig. 2. Elongational viscosity as a function of time at different strain rates at 180 °C.

short time. While at a higher extensional rate, the elongational viscosity grows up quickly at certain strain. The phenomenon is often called as strain hardening. Strain hardening behavior is very sensitive to the macromolecular structure, especially the long chain branches. This is a crucial property in many polymer processing's, such as thermoforming, blow molding and foaming [22]. In the case of foaming, strain hardening can prevent the melt from rupture and stabilize the bubbles. This is especially important for those polymers with low melt strength, such as polypropylene [8,9].

Fig. 2 shows the transient elongational viscosity of all samples at three elongational rates at 180 °C. It is found that there is no strain hardening in S0 at all elongational rate, which indicates a linear chain structure of S0. For the other samples, the strain hardening behavior is not obvious at low elongational rate. When the elongational rate is higher than 0.3 s^{-1}, these samples show significant strain hardening, which gives an unambiguous evidence of long chain branching. The higher the elongational rate is, the shorter the time is when nonlinearity happened. In addition, the samples reacted with higher content of PETA have higher elongational viscosity, which may be an evidence of a higher content of long chain branches. For quantitative estimation of the strain hardening effect, the so-called strain hardening coefficient S is determined [23]:

Table 2
Rheology parameters of the all samples from frequency sweep.

Sample	η_0 (Pa s)	λ (s)	n	Terminal slope of log G' α log ω
S0	4089.9	0.17	0.74	1.85
S2	7012.2	0.29	0.71	1.71
S3	8907.6	0.70	0.63	1.33
S5	15,050.8	1.85	0.59	0.88
S8	16,628.2	1.99	0.57	0.41

$$S = \frac{\eta_E^+(t,\dot{\varepsilon}_0)}{3\cdot\eta_0^+(t)} \tag{4}$$

where $\eta_0^+(t)$ is the time-dependent shear viscosity in the linear range of deformation and $\eta_E^+(t,\dot{\varepsilon}_0)$ the time-dependent elongational viscosity of samples. The higher the coefficient value, the stronger strain hardening behavior appears. In Fig. 3 the strain hardening coefficients at a total Hencky strain of 1 are shown as a function of elongational rate. It is much obviously proved that the sample reacted with higher content of PETA shows much stronger strain hardening behavior or higher melts strength. So the coefficient can be an indicator of strain hardening effect to connect sample rheological properties with foam structure.

Linear viscosity properties can also be used to prove the existence of long chain branching and the data can be used to quantitatively calculate the level of LCB. Tian et al. discussed those of long chain branched polypropylene in detail [14]. The results of long chain branched PS are similar to their work, so some data are just listed here to avoid repeat and detailed discussion can be found in the literature. Table 2 lists the rheological parameters fitted by Cross model and terminal slope of storage modulus. The presence of very low amounts of LCB can change the zero-shear viscosity (η_0) and the degree of shear shinning, as compared to the linear polymers. The increasing zero-shear viscosity from S0 to S8 indicates the increasing of LCB level. Besides zero-shear viscosity, the storage modulus (G') is even more sensitive to LCB. In the terminal zone, G' of linear polymers follows the well known frequency dependence [24], i.e.G' α ω^2. The terminal slope of sample S0 is close to 2 and exhibits typical terminal behavior, indicating the linearity of the molecular chain. The other samples deviate from this behavior. It can be seen that the slope decreased remarkably from S0 to S8. The non-terminal behavior of the samples reacted with PETA can be ascribed to the long chain branches.

To determine the LCB content, it is first assumed that the formed LCB structure is a three-arm star, which can be inferred from the

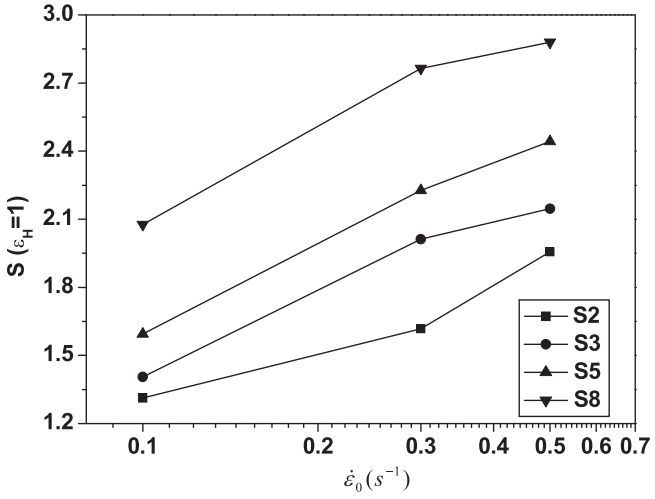

Fig. 3. Strain hardening coefficient S at Hencky strain of 1 as a function of strain rate $\dot{\varepsilon}_0$.

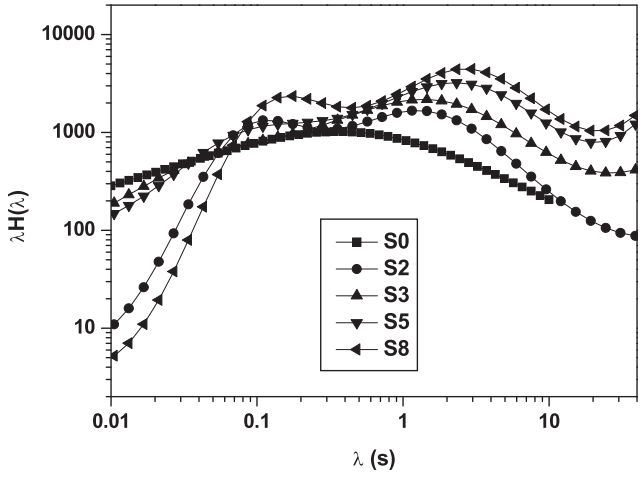

Fig. 4. Weighted relaxation spectra for all the samples.

Table 3
LCB level (x) of PETA-reacted samples and some corresponding rheological parameters used in calculations.

Sample	τ_L (s)	τ_B (s)	N_a	x	Number of branching point ($1/10^4$ C)
S2	0.12	1.30	5.1	0.055	0.15
S3	0.12	1.62	5.2	0.26	0.73
S5	0.12	2.36	5.4	0.56	1.56
S8	0.12	2.76	5.5	0.58	1.60

reactive mechanism [14,25]. The method used here is the same with that of Tian's [14] and the detailed calculation process can be found in their work. Here some results are just listed. First, a weighted relaxation spectrum (Fig. 4) can be calculated from the dynamic modulus data (not shown here) by GENEREG program [26]. From the spectra, it is found that S0 has only one relaxation time while the other samples have two. The shorter relaxation time (τ_L) of the PETA-reacted samples is close to that of S0, which can be ascribed to the relaxation of linear chain; while the longer relaxation time (τ_B) appears in these samples can be ascribed to the relaxation of branched chain. Then, the structural parameters, such as length of branches (N_a) and content of LCB PS (LCB level, x) in the sample, can be determined with the help of reptation model [25] for linear chains and Ball–McLeish model [27] for branched chains. The results are listed in Table 3, in which x is the fraction of the branched chains in all chains. From x, the number of branching point per 10^4 carbon atom on the backbone can also be calculated. It is found that the LCB level increases with the content of PETA; the increasing of branching chains length is very gentle and the improving of rheological properties is due to the increasing of number of branching point (or content of branching chains).

3.3. The influence of temperature on the foam structure

The effect of temperature on the foam structure was studied at a temperature range from 60 °C to 110 °C. A selection of SEM images of sample S3 foamed at constant pressure of 10 MPa is shown in Fig. 5, from which the large increase of cell size with temperature can be seen obviously. This is because higher temperature lowers the viscosity of the matrix and increases the diffusion rate of CO_2, both of which accelerate the growth of bubbles. On the other hand, it is well known that CO_2 can behave as a plasticizer which depresses the real T_g of polymer matrix. With the releasing of CO_2, T_g will increase until it reaches its

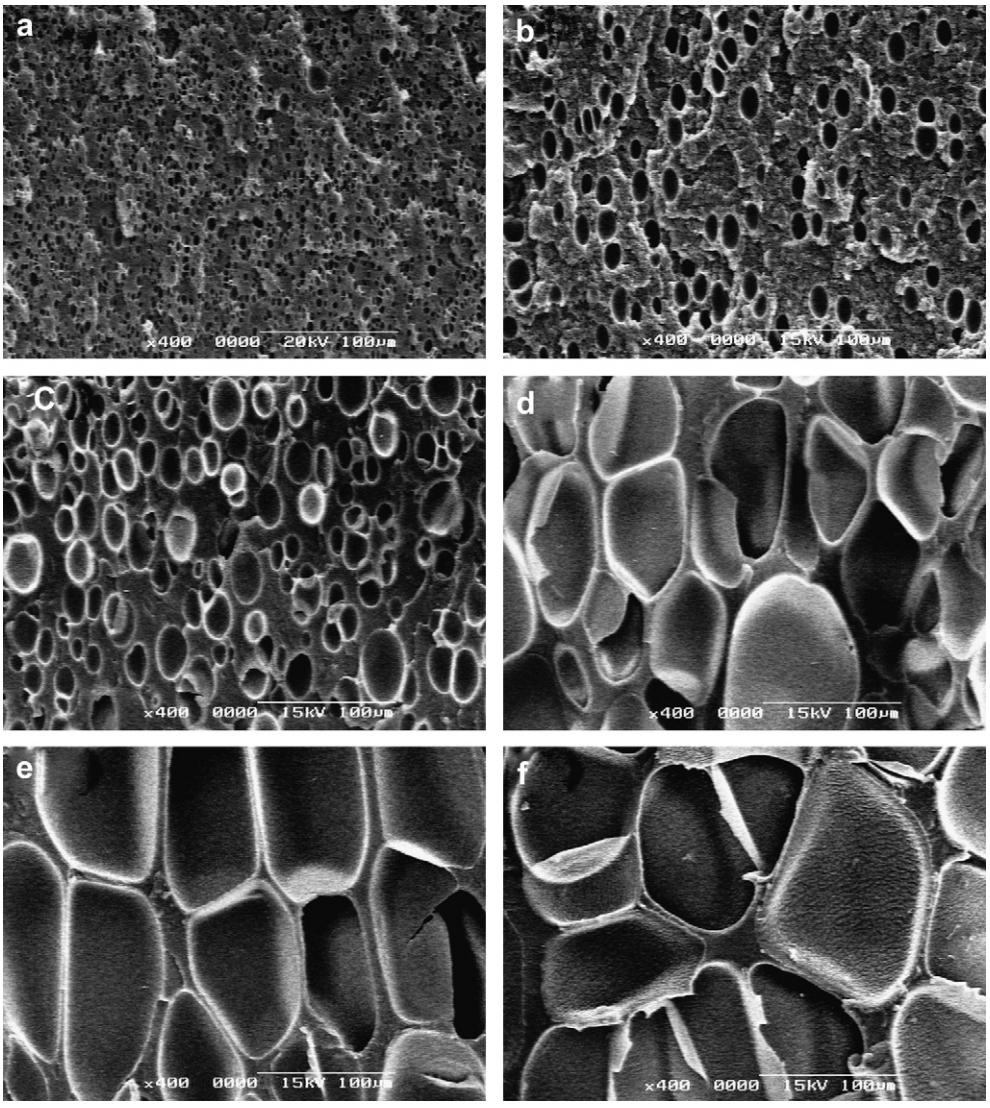

Fig. 5. SEM images of sample S3 foamed at 10 MPa and different temperatures: (a) 60 °C; (b) 70 °C; (c) 80 °C; (d) 90 °C; (e) 100 °C; (f) 110 °C. Magnification: 400×.

original value T_{g0}. Since the foaming temperatures chosen here are almost lower than T_{g0}, it will become lower than the actual T_g when the concentration of CO_2 in the system decreasing. Then the matrix cannot deform anymore and the foam structure is fixed. So the lower the foaming temperature chosen, the shorter time the cell can used to grow and at last the smaller the cell size is. The glass transition temperature of PS is around 106 °C, while the actual one under 10 MPa is about 72 °C according to Chow equation (see below for details). For the sample foamed at 110 °C, which is higher than T_{g0}, it has the biggest cells, even with certain rupture of the cells. The SEM images were analyzed to obtain the cell size distribution, average diameter and cell density. Fig. 6 illustrates the cell size distribution of S3 foamed at the same condition as that in Fig. 5. It is found that the distribution becomes broader with increasing foaming temperature. The cell size distribution is decided by both the nucleation and cell growth dynamics. Because the pressure is the same, the difference in nucleation may be insignificant. The time that the cells used to grow is the main reason for the difference of the cell size distribution. At low temperature, the actual glass temperature increases rapidly due to the decrease of CO_2 concentration as the cells grow up, which leaves relatively shorter time for the cell growth. While at temperature higher than T_{g0}, the cell growth cannot be stopped by the change of actual glass transition temperature.

The average cell diameter of all samples foamed at 10 MPa as a function of temperature is plotted in Fig. 7. For S3, foams with cell diameter from 5.8 μm to 167.7 μm are generated when the foaming temperature increases from 60 °C to 110 °C. On the contrary, the cell density decreases with temperature, which can be seen in Fig. 8. The cell density of S3 decreases from 5.88×10^{11} to 2.18×10^{5} cells/cm^3 at the same temperature range. From Fig. 7, it can be seen that the average diameter of all sample increases with temperature but the magnitude of increasing is different. At lower temperature, the diameter of all samples is very close; while at 110 °C, the diameter of S0 is almost four times to that of S8. The results show that the influence of LCB on cell size is more obvious at higher temperature than that at lower temperature. This is because that at lower foaming temperature (just a little higher than the T_g of polymer/CO_2 system), the viscosity of all samples is very close and controlled mainly by temperature, where the influence of long chain branching is not so obvious. At higher foaming temperature, the samples with higher LCB level have higher melt strength, leading to smaller cell size. It can be seen in Fig. 8 that the difference of cell density at higher foaming temperature is also greater than that at lower temperature.

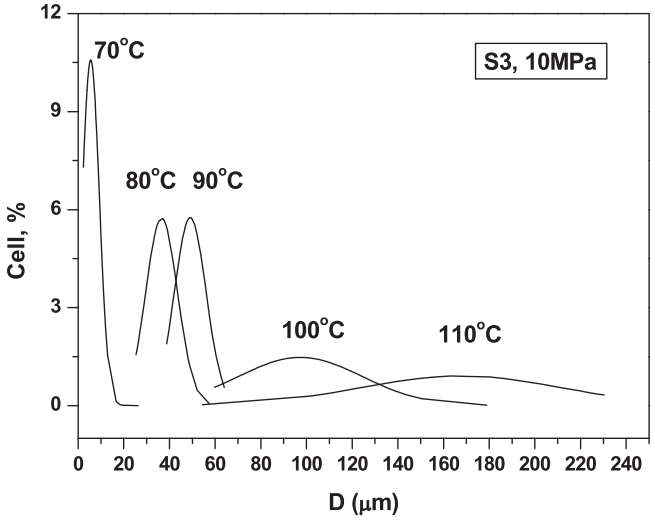

Fig. 6. Cell size distribution of sample S3 foamed at 10 MPa and different temperatures.

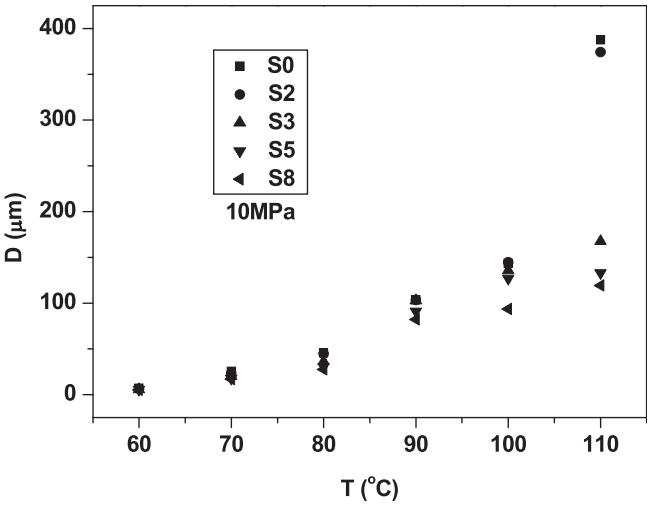

Fig. 7. Average cell diameter of all samples varied with temperature at 10 MPa.

3.4. The influence of pressure on the foam structure

The effect of the saturation pressure on the foam structure is studied at a constant temperature. Fig. 9 shows the SEM images of S8, from which the foam structure can be seen changing with pressure at 80 °C. It can be found intuitively that cell size decreases with pressure and the amount of cells increases with pressure. The cell size distributions at different pressure are shown in Fig. 10. It becomes narrower with increasing pressure, which means that more uniform foam structure can be obtained at higher pressure. This can be readily explained by classical nucleation theory [28]. At higher pressure, the nucleation rate is higher, so the amount of cells formed in a given volume and time is greater. Then these cells grow under same condition, resulting in a more uniform distribution. The cell size decreases with saturation pressure, which can be seen from Figs. 9 and 11. At lower saturation pressure, the energy barrier to nucleation is higher, so the amount of gas used to nucleate decreases and the gas used to cell grow increases, resulting in bigger cell size. The effect of pressure on the cell size seems saturate

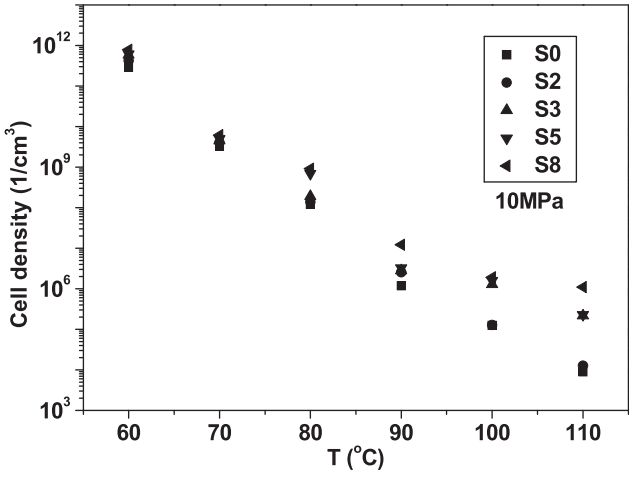

Fig. 8. Cell density of all samples varied with temperature at 10 MPa.

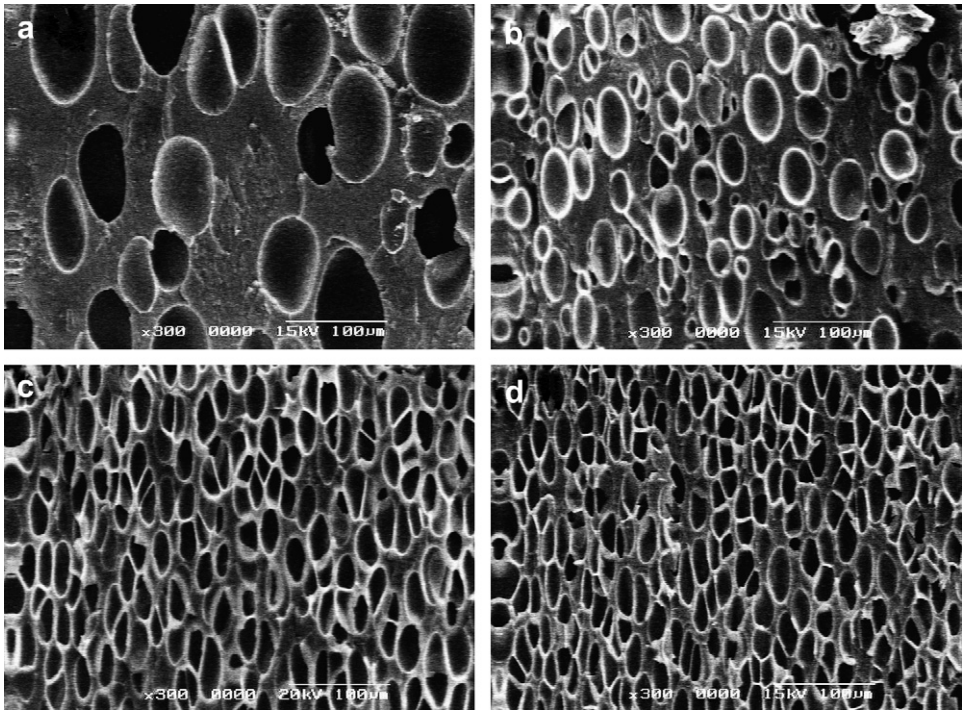

Fig. 9. SEM images of sample S8 foamed 80 °C and different pressures: (a) 8.6 MPa; (b) 10 MPa; (c) 12 MPa; (d) 14 MPa. Magnification: 300×.

at about 10 MPa, while the cell density increases continuously with pressure. The influence of LCB level on cell size is clearly shown in Fig. 11. At lower saturation pressure, the difference of cell size among samples is very obvious while that at higher saturation pressure is very small. It is believed that cell size is closely correlated with cell growth dynamics, which is a diffusion controlled process. At lower saturation pressure, the concentration of gas absorbed in polymer matrix is low, and the viscosity of the system doesn't drop greatly. Then the higher viscosity of samples with higher LCB level leads to a slow diffusion rate of gas. But at higher pressure, the viscosity decreases substantially because of higher content of gas absorption, which overwhelms the influence of LCB on viscosity. So the cell size difference at lower pressure is more obvious. The influence of pressure on cell density can be seen from Fig. 12. It is found that the cell density increases with saturation pressure. At higher pressure, the amount of CO_2 absorbed in the matrix is higher, so the amount of CO_2 used to nucleation would be higher and resulting in more cells. From classical nucleation theory [28], it is known that the energy barrier to nucleation decreases with the increasing of pressure drop, which leads to more cells being nucleated within a given volume at higher pressure. However, this process is not very closely related to the viscosity or modulus. Therefore, the influence of LCB level on cell density is not obvious when the foaming pressure changes.

3.5. The influence of LCB level on the foam structure

The SEM images of different samples foamed at 80 °C and 10 MPa are shown in Fig. 13. It is shown that the amount of ellipsoidal bubbles increases gradually from S0 to S8 and the diameter

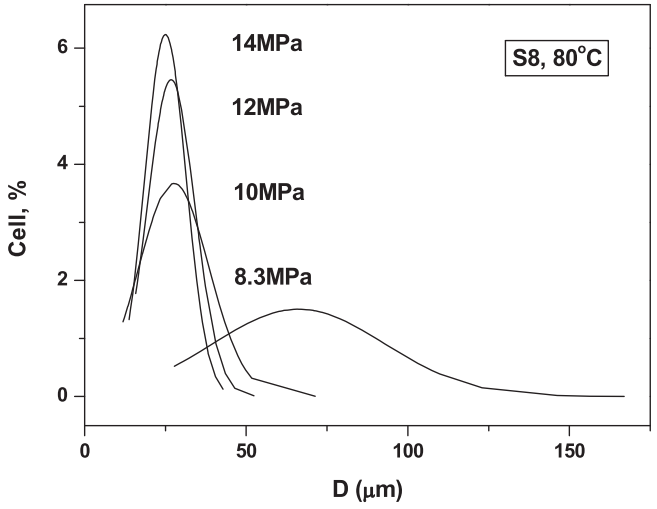

Fig. 10. Cell size distribution of sample S8 foamed at 80 °C and different pressures.

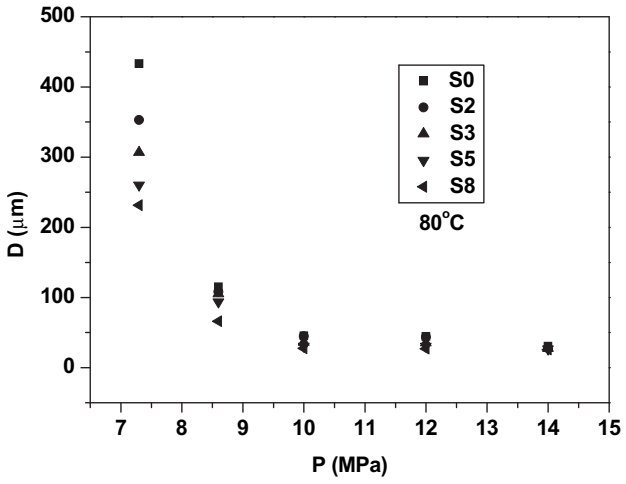

Fig. 11. Average cell diameter of all samples varied with pressure at 80 °C.

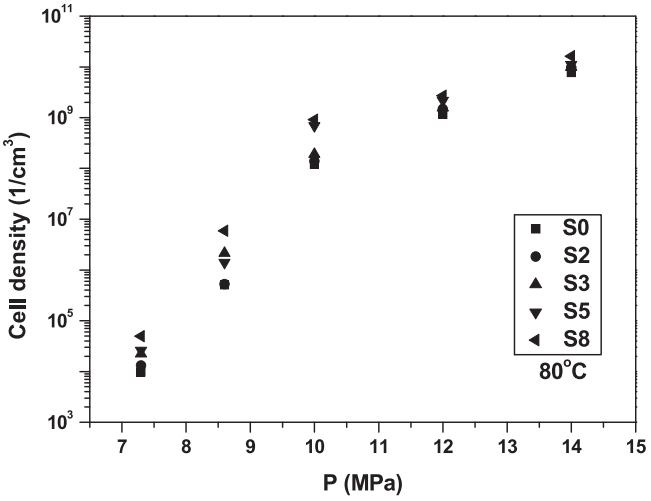

Fig. 12. Cell density of all samples varied with pressure at 80 °C.

changes on the opposite way. The cell size distributions for samples with different levels are plotted in Fig. 14. The average cell size decreases and the cell size distribution becomes narrower with increasing LCB level. The difference in cell size of the foam comes from the different nucleation time of cells. Cells that nucleate at early stage have longer time for cell growth. Long chain branched structures give rise to strain hardening at larger strain, which hinders the growth of cell in the late stage of foaming. So the difference between the cells formed at earlier time and later time would decrease, and the cell size distribution would become more uniform. Cell diameter and cell size distribution as a function of LCB level are plotted in Fig. 15. From this figure and the SEM images, it can be confirmed that the cell size decreases with *x* while the cell density increases with *x*. As can be seen in Figs. 2 and 3, the strain hardening behavior becomes much obvious with increasing LCB level. Under the same saturation pressure and pressure releasing rate, bubble growth dynamics of the branched sample that had higher entanglements would be severely hindered compared to the linear ones. So the branched samples have smaller cell size and higher cell density.

However, in most experiments, it is hard to know the chain topology clearly or to define the LCB level quantitatively. It is

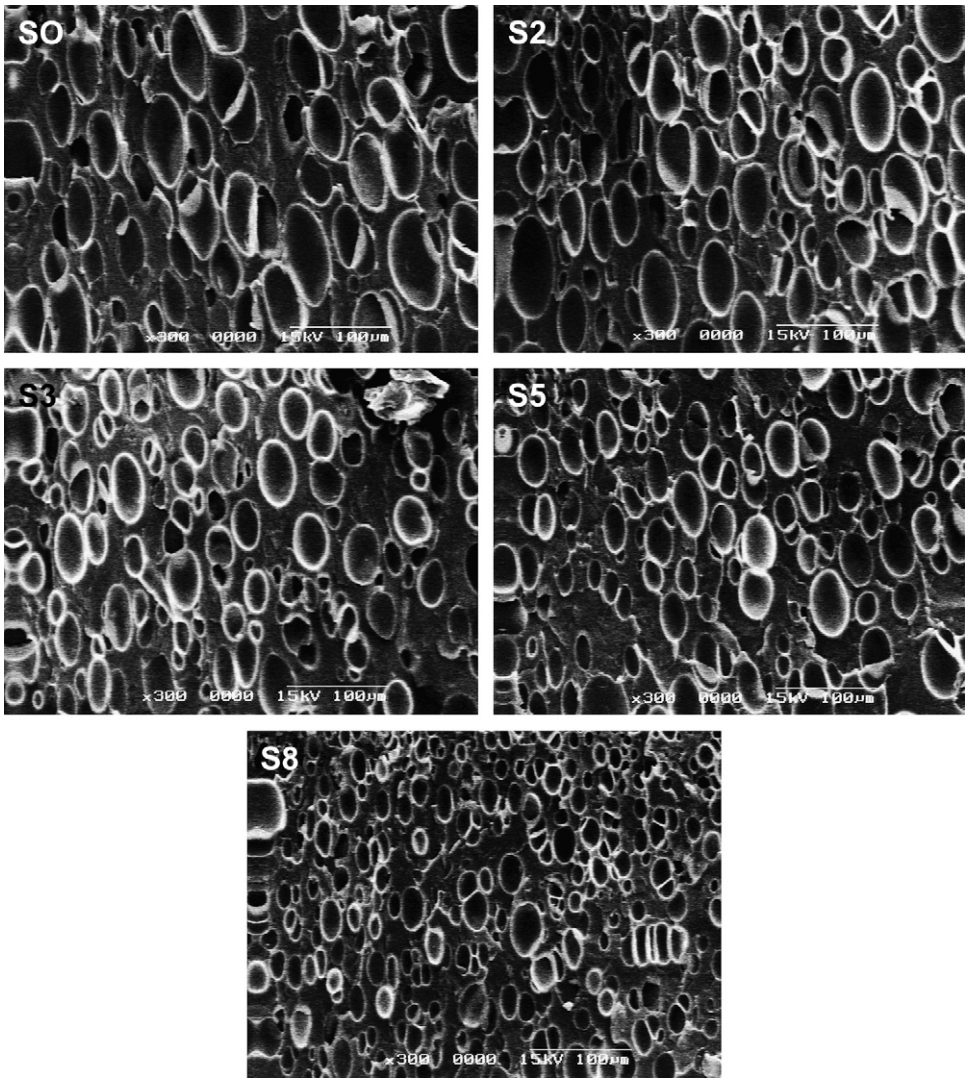

Fig. 13. SEM images of different samples foamed at 80 °C and 10 MPa. Magnification: 300×.

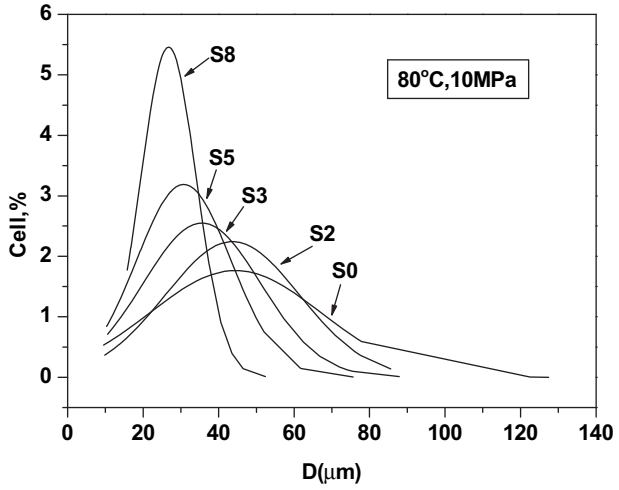

Fig. 14. Cell size distribution of all samples foamed at 80 °C and 10 MPa.

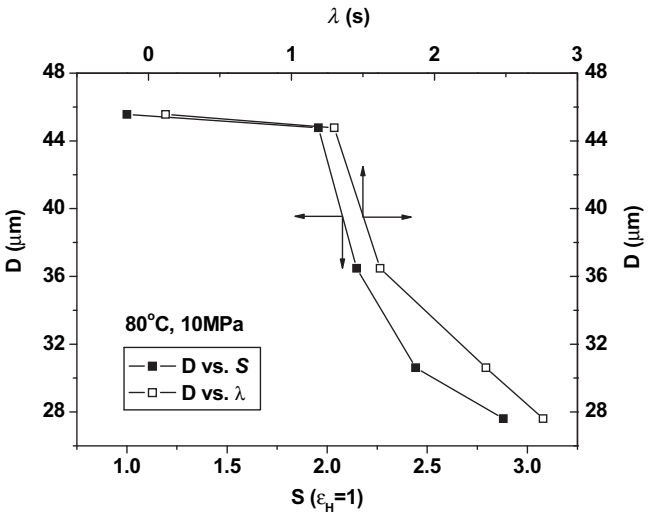

Fig. 16. The relationship among average cell diameter, strain hardening coefficient *S* and relaxation time λ. The value of *S* comes from Fig. 3 at elongational rate of 0.5 s^{-1}; λ is the maximum relaxation time in Table 3; the foaming condition was 80 °C and 10 MPa.

necessary to find a parameter that can be obtained easily to evaluate the foamability of a polymer. A possible try is the strain hardening coefficient *S*, which is closely related with the melt strength and can be a connection between the cell structures and the foamability of materials. The variation of average cell diameter as a function of *S* is shown in Fig. 16. When the value of *S* is smaller than 2, the cell diameter is very close at the foaming condition. That is to say, when *S* value of samples is small, the strain hardening behavior is not obvious, which leads to relatively larger cell diameter. With the increase of strain hardening coefficient, cell diameter decreases rapidly and the difference in the melt strength of sample manifests. By this method, the frequently used melt strength or elongational viscosity can be conveniently correlated with cell size of foams.

The maximum relaxation time can be also as a criterion for the variation of cell diameter, which is more correlative to molecular structure. For example, changing number of branching point, length of branching chain and increasing molecular weight etc. can alter the relaxation time. Fig. 16 simultaneously describes the average diameter of different sample changing with relaxation time. The trend of cell diameter varying with relaxation time is similar to that of strain hardening coefficient *S*. The variation of cell diameter is very gentle at small relaxation time, which is corresponding to low melt strength or low LCB level. The samples with small relaxation time have big cells, and the cell diameters are close to each other. With increasing relaxation time (because of long chain branching here), the cell diameter decreases quickly. On the other hand, although at most time the sample with shorter relaxation time can get the same cell diameter with that having longer relaxation time, the sample with longer relaxation time would have better cell structure. Fig. 17 shows the cell diameter of three samples foamed at 80 °C and different pressure as a function of relaxation time. At the same relaxation time, cell diameter decreases with pressure. The isobaric line means the samples foam under the same pressure. It can be speculated that three samples can have the same cell diameter at different pressure but with different cell density (because of different pressure). So the sample with longer relaxation time can get foams with big cells and higher cell density at the same time.

3.6. Simulations of foaming process

The above experimental results have shown that long chain branched molecules have great effects on the cell size, cell size

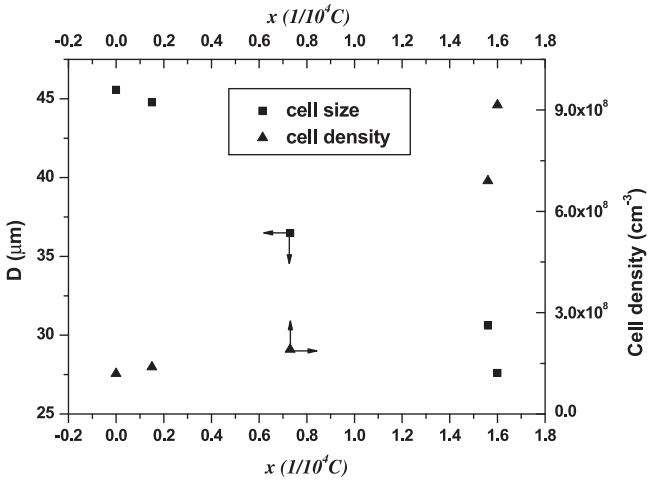

Fig. 15. Average cell diameter and cell density of samples foamed at 80 °C and 10 MPa varied with LCB level *x* (number of branching point per 10^4 carbon atom).

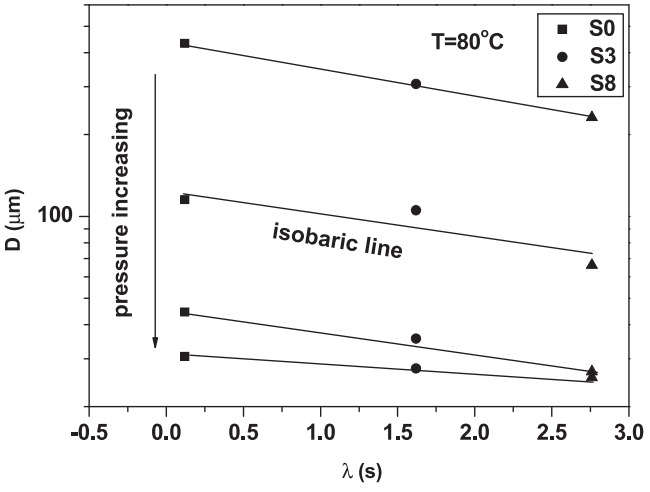

Fig. 17. Average cell diameter of samples foamed at 80oC and different pressure as a function of relaxation time (the arrow represented the pressure trend and the isobaric line denoted the sample foamed at the same pressure).

distribution and cell density. It also illustrates the effect of branch level with the same length of arm on the cell diameter. Although this is instructive for the design of molecular structures to get the desired foam materials, the experiments at present cannot cover all kinds of molecular structures. To do so, it is necessary to consider the problem theoretically. The model used to simulate bubble growth dynamics is the cell model that has been used in many works [9,10,12]. However, the difference between the present simulation and all previous ones are the connections between the molecular structures and the foam structures. In this paper, the following assumptions are made:

i. The bubble is spherically symmetric when it nucleates and remains so for the entire period of growth.
ii. The gas in the bubble follows the ideal gas law and is in thermodynamic equilibrium with the melt at the bubble surface. The equilibrium is described by Henry's law, $c(R,0) = k_H P_D(0) = \bar{c}(t')$
iii. The latent heat of solution and temperature changes upon expansion of gas in the bubbles is negligible, and the growth process can be considered as isothermal.
iv. The effect of gravity is neglected and the bubble remains stationary throughout its growth period.
v. Inertial effects are neglected and fluid is assumed to be incompressible.

Following the above assumptions, the bubble growth dynamics is described by the coupled mass and momentum conservation equations. The mass balance for gas in the bubble can be written as:

$$\frac{\mathrm{d}}{\mathrm{d}t}\left(\frac{4\pi}{3}\frac{R^3 P_D}{R_g T}\right) = 4\pi R^2 D\frac{\partial c}{\partial r}\bigg|_{r=R} \tag{5}$$

Mass balance for gas in melt is:

$$\frac{\partial c}{\partial t} + \frac{\dot{R}R^2}{r^2}\frac{\partial c}{\partial r} = \frac{D}{r^2}\frac{\partial}{\partial r}\left(r^2\frac{\partial c}{\partial r}\right) \tag{6}$$

The momentum equation in the polymers is:

$$P_D - P_C - \frac{2\gamma}{R} + 2\int_R^\infty \frac{\sigma_{rr}-\sigma_{\theta\theta}}{r}\mathrm{d}r = \frac{4\eta}{R}\left(\frac{\mathrm{d}R}{\mathrm{d}t}\right) \tag{7}$$

where R is the bubble radius, P_D the pressure in the bubble, P_C the ambient pressure, D the diffusion coefficient, c the gas concentration, η the viscosity, γ interfacial tension, T the temperature, R_g the gas constant, and σ the viscoelastic stress tensor. The influence of viscoelastic properties is taken into consideration by the normal stress difference $\sigma_{rr}-\sigma_{\theta\theta}$. The viscoelastic constitutive model used here is the Pom–Pom model, which is the only one that can connect the molecular structure with the nonlinear rheological properties [29–31]. In Pom–Pom model, the branched molecules have a backbone with molecular weight M_b, and both two ends of the backbone are connected to q arms with molecular weight M_a. The polydispersity in molecular structures will not be considered here. The stress tensor can be expressed as

$$\boldsymbol{\sigma} = \frac{15}{4}G_0\phi_b^\beta\lambda^2(t)\mathbf{S}(t) \tag{8}$$

which depends on the molecular orientation

$$\mathbf{S} = \mathbf{A}/tr\mathbf{A},\ \frac{D\mathbf{A}}{Dt} - \mathbf{K}\cdot\mathbf{A} - \mathbf{A}\cdot\mathbf{K}^T = -\frac{1}{\tau_b}(\mathbf{A}-\mathbf{I}) \tag{9}$$

and molecular stretch

$$\frac{D\lambda}{Dt}(t) = \lambda(t)\mathbf{K}:\mathbf{S} - \frac{1}{\tau_s}[\lambda(t)-1]e^{\nu^*(\lambda(t)-1)} \tag{10}$$

where D/Dt denotes material derivative, $\mathbf{K}$ is the velocity gradient tensor. Important time scales can be seen in Eq. (9) and (10), i.e., the backbone orientation relaxation time $\tau_b = 75/2\pi^2 s_b^2\phi_b^{2(\beta-1)}q\tau_a$ and the backbone stretch relaxation time $\tau_s = 5/2qs_b\phi_b^{\beta-1}\tau_a$. $\tau_a = \tau_0 e^{\nu^* s_a}$ is the relaxation time of arm. $s_a = M_a/M_e$ and $s_b = M_b/M_e$ (in which M_e is the average molecular weight between entanglements) are the dimensionless path lengths of arm and backbone, respectively, $\phi_b = M_b/2qM_a + M_b$ is the mass fraction of backbone. ν^* is a function of arm fraction ($= (15/4)\ 1-(1-\phi_a)^\beta \times (1+\beta\phi_a)/\beta(\beta+1)\phi_a^2$) and $\beta = 7/3$.

As for nucleation process, classical nucleation theory is used [12]. The nucleation rate can be written as:

$$J(t) = f_0\left(\frac{2\gamma}{\pi M_w/N_A}\right)^{1/2}\exp\left(-\frac{16\pi\gamma^3 F}{3k_B T(\bar{c}/k_H - P_C(t))^2}\right)N_A\bar{c}(t) \tag{11}$$

Normally, the denominator in the exponent term is $(P_D - P_C)$. P_D and P_C are changing with time, but in previous literatures, they often used the value of initial pressure of CO_2 and atmospheric pressure, respectively. This is right when the pressure release rate is very high. But in this experiment the pressure depression rate is limited (about 1 MPa/s). So P_D is replaced by $\bar{c}/k_H$ and $P_C(t)$ decreasing with time. This term reflects the influence of pressure depression rate.

The average concentration of gas dissolved in polymer melt at time t, $\bar{c}(t)$ is given by following equation:

$$\bar{c}(t)V_{L0} = c_0 V_{L0} - \int_0^t \frac{4\pi}{3}R^3(t-t',t')\frac{P_D(t-t',t')}{R_g T}J(t')V_{L0}\mathrm{d}t' \tag{12}$$

where V_{L0} is the volume of polymer matrix.

Eq. (5)–(12) can be solved simultaneously to get the cell size, cell size distribution and the cell density. However, it should be stressed that foaming process usually takes place under high pressure, high temperature and certain dissolved gas. All of these factors will affect the rheological properties substantially. For example, the effect of temperature can be considered by the time–temperature superposition principle, i.e., the viscosity can be written in a temperature independent form as

$$\frac{\eta(T)}{a_T(T)b_T(T)} \sim \dot{\gamma}a_T(T) \tag{13}$$

where $\dot{\gamma}$ is the strain rate, $a_T(T)$ and $b_T(T)$ are temperature dependent horizontal and vertical shift factor, respectively. $b_T(T)$ depends on the density difference under different temperatures, and is taken as one in many cases. $a_T(T)$ can be described by the WLF equation or Arrhenius equation depending on difference between the temperature and the glass transition temperature. It should be stressed that both viscosity and the relaxation time can be shifted if the temperature changes. The effect of pressure can also be simply considered as

$$\frac{\eta(P)}{a_P(P)b_P(P)} \sim \dot{\gamma}a_P(P) \tag{14}$$

$a_P(P)$ and $b_P(P)$ are pressure dependent horizontal and vertical shift factor, respectively. Similarly, vertical shift factor $b_P(P)$ is usually ignored and the horizontal factor $a_P(P)$ can be expressed as $a_P(P) = e^{\beta'(P-P_0)}$, where β' is a constant and P_0 is the reference pressure.

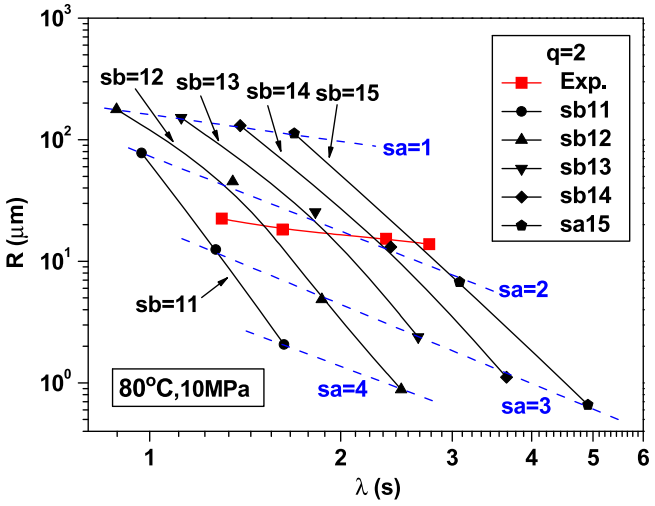

Fig. 18. The simulated radius with different length of arm and backbone length varies with relaxation time. The solid square (■) represents the experimental results that performed at the same pressure of 10 MPa and temperature of 80 °C. The other solid symbols represent the simulated results of temperature at 80 °C. The data on solid line show the results of the same backbone length but different arm length, and the dash line is just on the opposite way.

The effect of gas is usually considered together with the effect of pressure. It has been shown that a similar master curve can be obtained via [32]

$$\frac{\eta(P,c)}{a_{P,c}(P,c)b_{P,c}(P,c)} \sim \dot{\gamma} a_{P,c}(P,c) \tag{15}$$

The shift factors depend on the pressure and the gas concentration simultaneously. To simplify the problem, it is usually to assume the effect of pressure and the gas concentration can be separated, which suggests $a_{P,c}(P,c) \approx a_P(P)a_c(c)$ and $b_{P,c}(P,c) \approx b_P(P)b_c(c)$. The effect of gas concentration on vertical shift will not be considered here. The key problem is to calculate the gas effect on horizontal shift factor $a_c(c)$, which can be expressed by the combination of the Chow equation [33] and the WLF equation [34].

$$\log a_c(c) = \log \frac{\eta}{\eta_g} = -\frac{c_1[T - T_g(c)]}{c_2 + T - T_g(c)} \tag{16}$$

$$\ln\left(\frac{T_g}{T_{g0}}\right) = \psi[(1-\theta)\ln(1-\theta) + \theta \ln \theta], \quad \theta = \frac{w/M_{w1}}{z(1-w)/M_{w2}}, \quad \psi = \frac{zR_g}{M_{w2}\Delta C_p} \tag{17}$$

where c_1 and c_2 are constants, $T_g(c)$ is the glass transition temperature depending on the gas concentration, w is the weight fraction of gas, M_{w1} and M_{w2} are the molecular weight of gas and polymer respectively, ΔC_p is the change of specific heat at T_g and z is a constant [31]. The effects on the gas diffusion coefficients and the interfacial tension are also considered, however, their contributions are not significant.

The control equations, the constitutive equations, the nucleation theory and the effects of temperatures, pressures, and gas concentrations can be solved simultaneously to get the foam structures. The detail calculation procedures are similar to that of Taki [12] except the viscoelastic model is used and finite element method is used to solve the bubble growth problem. The main parameters used in calculation are listed in Table 3.

Fig. 18 shows the calculated radius with different backbone length (S_b) and arm length (S_a) varying with relaxation time at 80 °C and 10 MPa. The length of arm used to calculate is in the range of 1–4 M_e while that of backbone is in the range of 11–15 M_e. The number of arm on each branching point (q) is 2. With these data and Pom–Pom model, the relaxation time of each topological structure can be calculated. It is assumed that the backbone orientation relaxation time in Pom–Pom model could be compared with the longer relaxation time in relaxation spectra (Fig. 4 and Table 4) calculated from frequency sweep data. It can be seen that the simulation results are in good agreement with experimental data. From simulation results, it is found that the radius decreases with the increase of backbone and arm length. This is due to the increase of viscosity and elasticity with increasing backbone or arm length. Important information from the simulation results is that arm length has greater influence on bubble radius than backbone

Table 4
The parameters used in the calculation.

	Parameter	Value	Unit	Refs.
Physical properties	Solubility constant, K_H[a]	1.66×10^{-4}	mol-gas/m^3/Pa	[35]
	Surface tension, γ_0	27.4×10^{-3}	N/m	[34]
	Diffusion coefficient, D_0	7.48×10^{-9}	m^2/s	[34]
	T_g of polymer under air pressure, T_{g0}	379.15[b]	K	
	Specific heat change of polymer, ΔC_P	295[b]	J/Kg/K	
	Molecular mass of foaming agent, M_g	44×10^{-3}	Kg/m^3	
	Molecular mass of polymer monomer, M_P	104×10^{-3}	Kg/m^3	
	Density of polymer, ρ	1050	Kg/m^3	
Nucleation parameters	Correction factor of Zeldovich factor, f_0	3.5×10^{-28}		[12]
	Correction factor of free energy barrier, F	0.014		[12]
	Threshold of bubble nucleation, J_s	9.8×10^6	1/s/m^3	[12]
Pom–Pom model parameters	Pom–Pom model parameter, β	7/3		[31]
	Pom–Pom model parameter, α	0.01		[31]
	Modulus at T_r, $G_0\_T_r$[c]	2×10^5	Pa	[36]
	Newtonian viscosity at T_r, $\eta_s\_T_r$	2796	Pa s	[37]
WLF-Chow model	WLF model parameter, c_1	13.7		[34]
	WLF model parameter, c_2	50		[34]
	Chow model parameter, z	2		[33]
	Pressure coefficient, β_P	220×10^{-12}		[32]
Constant	Gas constant, R_g	8.314	J/mol/K	
	Avogadro constant, N_A	6.02×10^{23}	1/mol	
	Boltzmann constant, k_B	1.38×10^{-23}	J/K	

[a] The calculation of K_H is corresponding to equation $\ln(K_H) = 6.498 + 2.380(T_C/T)^2$ [35] at temperature of 80 °C and pressure of 10 MPa.
[b] From Experiment data.
[c] $T_r = 180$ °C.

length. A much stronger dependence of cell size on the variation of arm length than the change of backbone length is clearly shown. Although the backbone length has greater effect on the maximum relaxation time of polymers, changing the arm length is more efficient to control the cell size. As we know, this is the first report that arm length has greater influence on bubble radius than backbone length. From Fig. 18, it can be seen that the decreasing trend of experimental radius is much gentle as compared to the simulation results with constant backbone length and varying arm length, but quite close to the results with constant arm length and varying backbone length. In fact, from the free radical reaction mechanism, the long chain branching PS used in experiments could be regarded as a mixture of linear polymer and three-armed star polymer. The increasing of relaxation time is attributed to the increasing fraction of long chain branched polymer, but arm length is almost unchanged. The consistency of experiments and simulations partially justifies the results of simulation.

Fig. 19 shows the simulation results of cell density compared with experimental results. Although the calculated values are smaller than the corresponding experimental results, the trend of calculated results is the same to that of experiments. That is to say, under higher foaming pressure, the foam has higher cell density. The influence of arm or backbone length on cell density is not obvious here. This was also true for experiments, which showed only slightly increase of cell density with the increase of LCB level or the relaxation time. According to the nucleation equation, the nucleation rate of cell density is closely related with interfacial tension and foaming pressure. But the interfacial tension of samples with different chain length is almost the same. Therefore, the calculated cell density changes with CO_2 pressure but are insensitive to chain structure.

From the simulation results, especially from Fig. 18, some useful prediction can be made. On the one hand, for a certain LCB polymer, after the rheology properties are known, the approximate cell diameter and cell density under a certain foaming condition can be speculated. On the other hand, it can be used to suggest the foaming condition or rheological properties of polymer melts. For example, if one wants to get submicron foams, it can be expected that the maximum relaxation time of the polymer should longer than 2 s, and the topology of polymer chains requires a longer arm. For those want to make millimeter foams, higher temperature, longer backbone and shorter arm length are recommended.

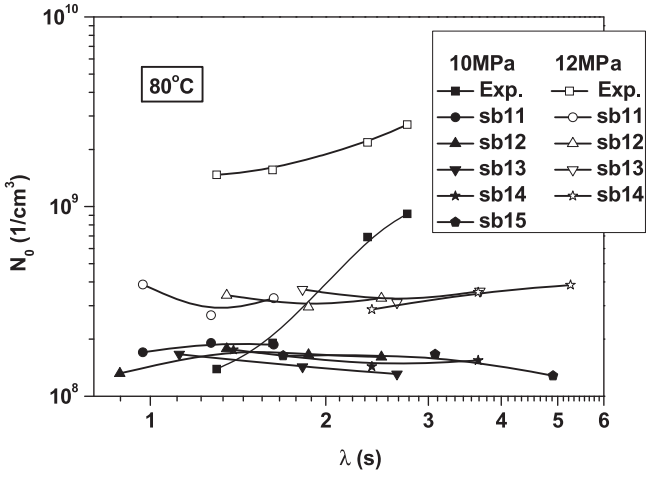

Fig. 19. The calculated cell density compared with that foamed at the same temperature of 80 °C and different pressure of 10 MPa and 12 MPa. The solid and hollow square (■, □) represents the experimental results that foamed under 10 MPa and 12 MPa, respectively. The solid symbols represent the calculated cell density under 10 MPa, while the hollow symbols represent that under 12 MPa.

4. Conclusions

The relationship between rheological properties and foam structure (cell size, cell density and cell size distribution) was investigated by foaming of LCB PS samples (that had different rheological properties) with $scCO_2$ as physical foaming agent. The effect of rheology on the foam structures were studied by tuning the chain structures of PS, with the LCB level ranged from 0 of S0 to 1.6 branching points per 10^4 carbon atoms on backbone of S8. The modified samples exhibited different rheological properties both in shear and elongational flow, with obvious strain hardening behavior. The foam structures were strongly dependent on the foaming conditions as well as the chain structures. The cell size increased with temperature while the cell density decreased with temperature. The influence of LCB level on cell size was not obvious at lower foaming temperature, while the difference of cell size among samples with different LCB level increased with foaming temperature. The cell size distribution became broader with increasing foaming temperature. But the saturation pressure had different influence on the foam structure. The cell size decreased and cell density increased with increasing of saturation pressure, which was the result of decreasing of the energy barrier to nucleation. The cell density of samples with different LCB level was close at each saturation pressure, but the samples with higher LCB level had smaller cell size at lower pressure. As for long chain branching structures, the increased elongational viscosity, complex viscosity and storage modulus with LCB level slowed down the growth rate of cells. This leaded to the decreasing of cell size, increasing of cell density and uniformity of cell size distribution at a given temperature and pressure.

The influences of molecular topology, especially the length of backbone and arm, on foam structure were further investigated by simulations. Pom–Pom model was used to describe the rheological properties of model branched polymer. Simulation results showed a quite different dependence of cell radius on the arm length and backbone length. It seemed that variation of arm length could be a method to control the cell size efficiently. However, the influence of branching level on the calculated cell density was not as obvious as experimental values. The simulation results were partially justified by the experimental results with constant arm length and increasing branching level. It can be concluded from the experimental results and the numerical simulation that the foam structures of amorphous polymer can be tuned by its rheological properties or molecular structures. Control on the rheology or molecular structure of polymers can extend the possible foam structures than that might be obtained under different processing conditions.

Acknowledgement

This work is supported by Natural Science Foundation of China (NSFC) no 50390095. Thanks to associated Professor Tao Liu and Dr. Xiulei Jiang from East China University of Science and Technology for HPDSC measurements. Thanks to Ms. Weixia Yan from Donghua University for the elongational rheology experiments.

References

[1] Reverchon E, Cardea S. J Supercrit Fluids 2007;40:144–52.
[2] Arora KA, Lesser JA, McCarthy TJ. Macromolecules 1998;31:4614–20.
[3] Stafford CM, Russell TP, McCarthy TJ. Macromolecules 1999;32:7610–6.
[4] Di Y, Iannace S, Maio ED, Nicolais L. Macromol Mater Eng 2005;290:1083–90.
[5] Lee LJ, Zeng C, Cao X, Han X, Shen J, Xu G. Compos Sci Technol 2005;65:2344–63.
[6] Di Y, Iannace S, Maio ED, Nicolais L. J Polym Sci Part B Polym Phys 2005;43:689–98.
[7] Nam GJ, Yoo JH, Lee JW. J Appl Polym Sci 2005;96:1793–800.
[8] Gotsis AD, Zeevenhoven BLF, Hogt AH. Polym Eng Sci 2004;44:973–82.

[9] Shafi MA, Flumerfelt RW. Chem Eng Sci 1997;52:626–33.
[10] Shafi MA, Joshi K, Flumerfelt RW. Chem Eng Sci 1997;52:635–44.
[11] Joshi K, Lee GJ, Shafi MA, Flumerfelt RW. J Appl Polym Sci 1998;67:1353–68.
[12] Taki K. Chem Eng Sci 2008;63:3643–53.
[13] Montminy MD, Tannenbaum AR, Macosko CW. J Colloid Interface Sci 2004;280:202–11.
[14] Tian J, Yu W, Zhou C. Polymer 2006;37:7962–9.
[15] Moad M. Prog Polym Sci 1999;24:81–142.
[16] Ratzsch M, Arnold M, Borsig E, Bucka H, Reichelt N. Prog Polym Sci 2002;27:1195–282.
[17] Graebling D. Macromolecules 2002;35:4602–10.
[18] Shroff RN, Mavridis H. Macromolecules 2001;34:7362–7.
[19] Wood-Adams PM, Dealy JM, deGroot AW, Redwine OD. Macromolecules 2000;33:7489–99.
[20] Kurzbeck S, Oster F, Munstedt H, Nguyen TQ, Gensler R. J Rheol 1999;43:359–74.
[21] Wagner MH, Bastian H, Hachmann P, Meissner J, Kurzbeck S, Munstedt H, et al. Rheol Acta 2000;39:97–109.
[22] Weng W, Markel EJ, Dekmezian AH. Macromol Rapid Commun 2001;22:1488–92.
[23] Stange J, Uhl C, Münstedtb H. J Rheol 2005;49:1059–79.
[24] Ruymbeke E, Stphenne V, Daoust D, Godard P, Keunings R, Bailly C. J Rheol 2005;49:1503–20.
[25] Tsenoglou CJ, Gotsis AD. Macromolecules 2001;34:4685–7.
[26] Roths T, Marth M, Weese J, Honerkamp J. Comput Phys Commun 2001;139:279–96.
[27] Garcia-Franco CA, Srinivas S, Lohse DJ, Brant P. Macromolecules 2001;34:3115–7.
[28] Goel SK, Beckman EJ. Polym Eng Sci 2004;34:1137–47.
[29] McLeish TCB, Larson RG. J Rheol 1998;42:81–110.
[30] Blackwell RJ, McLeish TCB, Harlen OG. J Rheol 2000;44:121–36.
[31] Verbeeten WMH, Peters GWM, Baaijens FPT. J Rheol 2001;45:823–43.
[32] Park HE, Dealy JM. Macromolecules 2006;39:5438–52.
[33] Chow TS. Macromolecules 1980;13:362–4.
[34] Chen X, Feng JJ, Bertelo CA. Polym Eng Sci 2006;46:97–107.
[35] Sato Y, Fujiwara K, Takikawa T, Sumarno, Takishima S, Masuoka H. Fluid Phase Equilib 1999;162:261–76.
[36] Liu C, He J, Ruymbeke Ev, Keunings R, Bailly C. Polymer 2006;47:4461–79.
[37] Dullaert K, Mewis J. J Colloid Interface Sci 2005;287:542–51.